

## WW Scattering

---

**Saurabh D. Rindani\***

*Physical Research Laboratory, Ahmedabad*

*E-mail: saurabh@prl.res.in*

The scattering amplitude of massive gauge bosons can be large at energies below the scale of the Higgs mass in theories where the gauge bosons get their mass by the Higgs mechanism. This would lead to a strongly interacting gauge sector. In general, the scattering of longitudinally polarized massive gauge bosons can give information on the mechanism of spontaneous symmetry breaking. At energies below the symmetry breaking scale, the equivalence theorem relates the scattering amplitudes to those of the “would-be” Goldstone modes. In the absence of Higgs bosons, unitarity would be restored by some new physics which can be studied through  $WW$  scattering. An example of Higgsless models is discussed. Isolating  $WW$  scattering at a hadron collider from other contributions involving  $W$  emission from parton lines needs a good understanding of the backgrounds. It has been found that for no kinematic cuts does the  $WW$  scattering contribution give a dominant contribution. The equivalent vector-boson approximation also has been found to overestimate the cross section and the  $WW$  invariant mass distribution. A study of the full  $WW$  production process in the region of high invariant  $WW$  mass can nevertheless serve to distinguish models with light and heavy Higgs bosons.

*From Strings to LHC*

*January 2-10, 2007*

*Goa, India*

---

\*Speaker.

## 1. Introduction

Amplitudes for scattering in theories with massive spin-1 particles can have bad high-energy behaviour. The propagator for a massive spin-1 field has a term which does not decrease with increasing momentum, leading to bad high-energy behaviour in amplitudes involving exchange of these vector particles. This can make the theory non-renormalizable. In theories with spontaneous symmetry breaking, renormalizability is maintained because Higgs exchange can cancel the bad high-energy behaviour arising from vector exchange. Amplitudes with massive vector particles in the initial and final states have bad high-energy behaviour because the polarization vector has the form

$$\epsilon_L^\mu(k) \approx \frac{k^\mu}{m_V}. \quad (1.1)$$

Scattering of longitudinally polarized gauge bosons would have the largest amplitudes at high energy. Again, if the mass of the vector fields arises through a Higgs mechanism, the bad high-energy behaviour is cured. However, if the Higgs mass is too high ( $s \ll m_H^2$ ), the amplitude can be large, leading to a strongly-interacting gauge sector. The study of  $WW$  scattering can thus be important in studying the mechanism of symmetry breaking.

Vector-boson scattering amplitudes at high energies may be calculated using the equivalence theorem [1]. The equivalence theorem relates the  $W_L W_L$  scattering amplitude to the amplitude for scattering of the corresponding “would-be” Goldstone scalars at high energy ( $s \gg m_W^2$ ). (Note that henceforth, unless clear from the context,  $W$  would refer to both  $W$  and  $Z$ ). Thus,

$$\begin{aligned} M(W_L W_L \rightarrow W_L W_L) &= M(w w \rightarrow w w) \\ M(Z_L Z_L \rightarrow Z_L Z_L) &= M(z z \rightarrow z z) \\ M(W_L Z_L \rightarrow W_L Z_L) &= M(w z \rightarrow w z) \\ M(W_L W_L \rightarrow Z_L Z_L) &= M(w w \rightarrow z z), \end{aligned} \quad (1.2)$$

where  $w$  and  $z$  are respectively the scalar modes which provided the longitudinal modes for  $W$  and  $Z$  respectively.

Goldstone boson interactions are governed by low-energy theorems for energy below the symmetry breaking scale ( $s \ll m_{\text{SB}}^2$ ). Low-energy theorems are analogous to those obtained for  $\pi\pi$  scattering in the chiral Lagrangian [2]. Thus, when there is no light Higgs (with  $m_H < 1$  TeV or so), the low-energy theorems combined with equivalence theorem can predict  $W_L W_L$  scattering amplitudes from the symmetries of the theory to leading order in  $s/m_{\text{SB}}^2$ . The specific theory for symmetry breaking then shows up at the next higher order in  $s/m_{\text{SB}}^2$ .

In the standard model (SM), we have the relations

$$m_H^2 = -2\mu^2 = 2\lambda v^2 = \lambda\sqrt{2}/G_F, \quad (1.3)$$

where  $\lambda$  is the quartic scalar coupling, and  $\mu$  is the mass parameter in the scalar potential.  $v$  is the vacuum expectation value of the neutral Higgs. Since  $v$  and  $G_F$  are fixed from experiment, large  $m_H$  means large  $\lambda$ . For  $m_H \gtrsim (G_F/\sqrt{2})^{-1}$ , perturbation theory is not valid. This corresponds to  $m_H \approx 300$  GeV.

A limit may be obtained from unitarity, if the tree amplitudes are to be valid at high energies. The Higgs cannot be very heavy, or else the unitarity limit would be crossed too soon. To see this,

write the old-fashioned scattering amplitude  $f_{cm}$ , so that  $|f_{cm}|^2 = \frac{d\sigma}{d\Omega}$ . Then we have

$$f_{cm} = \frac{1}{8\pi\sqrt{s}} \mathcal{M}. \quad (1.4)$$

The scattering amplitude has the partial wave expansion

$$f(\theta) = \frac{1}{k} \sum_l (2l+1) P_l(\cos\theta) a_l, \quad (1.5)$$

where  $a_l = e^{i\delta_l} \sin\delta_l$  is the partial wave amplitude written in terms of the phase shift  $\delta_l$ . Unitarity is expressed by the optical theorem relation

$$\sigma = (4\pi/k) \text{Im}f(0). \quad (1.6)$$

For elastic scattering, the phase shift  $\delta_l$  is real, but has a positive imaginary part if there is inelasticity. A convenient way to express elastic unitarity is

$$\text{Im}[a_l^{-1}] = -1. \quad (1.7)$$

From this it follows that

$$|a_l| \leq 1; \quad |\text{Re}a_l| \leq \frac{1}{2}. \quad (1.8)$$

The  $l=0$  partial-wave unitarity for large  $s$  for WW scattering then gives

$$m_H^2 < \frac{4\sqrt{2}\pi}{G_F}. \quad (1.9)$$

This gives a limit of  $m_H < 1.2$  TeV. Similar limits may be obtained by considering other partial-wave channels.

## 2. $W_L W_L$ scattering beyond Higgs mechanism

Violation of unitarity may be prevented in different ways, depending on the model. Models can have extra fermions and extra gauge interactions, which give additional contributions to  $W_L W_L$  scattering, e.g., resonances. An example is the techni-rho resonance in techni-color models, or new massive vector bosons (MVB's) in Higgsless models, A no-resonance scenario is described in an electro-weak chiral Lagrangian (EWCL) model, where one writes effective bosonic operators [3]. Unitarization can be built in by the use of Padé approximants or the K-matrix method and this can generate a resonant behaviour [4].

Terms in the chiral lagrangian must respect (spontaneously broken)  $SU(2)_L \times U(1)$  gauge symmetry. Experiment demands that the Higgs sector also approximately respect a larger  $SU(2)_L \times SU(2)_C$  symmetry, though the  $SU(2)_C$  custodial symmetry is broken by the Yukawa couplings and the  $U(1)$  gauge couplings. The chiral lagrangian is thus constructed using the dimensionless unitary unimodular matrix field  $U(x)$ , which transforms under  $SU(2)_L \times SU(2)_C$  as  $(2, 2)$ . Pieces of the chiral Lagrangian in the  $M_H \rightarrow \infty$  limit of the linear theory at tree level are:

$$\mathcal{L}_0 \equiv \frac{1}{4} f^2 \text{Tr}[(D_\mu U)^\dagger (D^\mu U)] - \frac{1}{4} B_{\mu\nu} B^{\mu\nu} - \frac{1}{2} \text{Tr} W_{\mu\nu} W^{\mu\nu}, \quad (2.1)$$

An additional dimension-two operator allowed by the  $SU(2)_L \times U(1)$  symmetry:

$$\mathcal{L}'_1 \equiv \frac{1}{4} \beta_1 g^2 f^2 [Tr(TV_\mu)]^2. \quad (2.2)$$

This term, which does not emerge from the  $M_H \rightarrow \infty$  limit of the renormalizable theory at tree level, violates the  $SU(2)_C$  custodial symmetry even in the absence of the gauge couplings. It is the low energy description of whatever custodial-symmetry breaking physics exists, and has been integrated out, at energies above roughly  $\Lambda_\chi \equiv 4\pi f \simeq 3\text{TeV}$ . At tree level,  $\mathcal{L}'_1$  contributes to the deviation of the  $\rho$  parameter from unity.

At the dimension-four level, there are a variety of new operators that can be written down. Making use of the equations of motion, and first restricting attention to CP-invariant operators, the list can be reduced to eleven independent terms [3].

In EWCL, one can build in unitarity at a given order by using a non-perturbative modification, which reduces to the original amplitude at the perturbative level [4]. One writes a low-energy expansion as  $a(s) = a^{\text{LET}}(s) + a^{(1)}(s)$ . At the lowest order Padé approximant gives

$$a^{\text{Padé}}(s) = \frac{a^{\text{LET}}(s)}{1 - \frac{a^{(1)}(s)}{a^{\text{LET}}(s)}}. \quad (2.3)$$

The  $K$  matrix method gives

$$a^K(s) = \frac{a^{\text{LET}}(s) + \text{Re}a^{(1)}(s)}{1 - i(a^{\text{LET}}(s) + \text{Re}a^{(1)})}. \quad (2.4)$$

Both satisfy unitarity by construction to the relevant order.

## 2.1 Higgsless models

A number of Higgsless models have been proposed recently [5, 6]. In these models, symmetry breaking is achieved by appropriate boundary conditions. The models differ in spatial dimensions, 5 in the original versions, 4 in the "deconstructed" versions. They also differ in embedding of SM fermions. New weakly coupled particles appear at TeV scale and postpone unitarity violation. A version of the model with modified fermion sector can raise the scale of unitarity violation by at least a factor of 10 without running into conflict with precision electroweak constraints.

In the absence of Higgs, new massive vector boson propagators contribute to  $WW$  scattering. The bad high energy behaviour of  $WZ$  scattering, for example, is cancelled by the contribution of the MVBs because of coupling constant sum rules:

$$g_{WWZZ} = g_{WWZ}^2 + \sum_i (g_{WZV}^{(i)})^2, \quad (2.5)$$

$$2(g_{WWZZ} - g_{WWZ}^2)(M_W^2 + M_Z^2) + g_{WWZ}^2 \frac{M_Z^4}{M_W^2} = \sum_i (g_{WZV}^{(i)})^2 \left[ 3(M_i^\pm)^2 - \frac{(M_Z^2 - M_W^2)^2}{(M_i^\pm)^2} \right]. \quad (2.6)$$

Unitarity is violated at a scale

$$\Lambda \approx \frac{3\pi^4}{g^2} \frac{M_W^2}{M_1^\pm} \approx 5 - 10 \text{ TeV}. \quad (2.7)$$

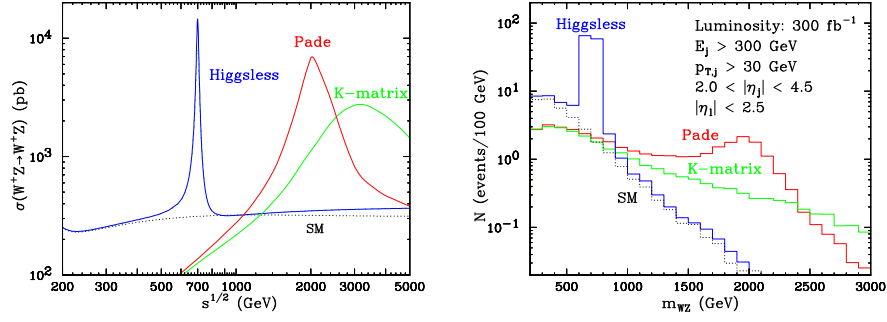


**Figure 1:** Signal and background cross-sections (in fb) and significance for  $M_V = 700$  GeV for the  $pp$  collider at the LHC with center-of-mass energy  $\sqrt{s} = 14$  TeV and a total integrated luminosity of  $300 \text{ fb}^{-1}$ . The effect of various cuts on the cross-sections is shown. (From [7])

The first MVB should appear below 1 TeV, and thus accessible at LHC. In the approximation that the first state  $V_1$  saturates the sum rules, its partial width is given by

$$\Gamma(V_1^\pm \rightarrow W^\pm Z) \approx \frac{\alpha(M_1^\pm)^3}{144s_W^2 M_W^2}. \tag{2.8}$$

For  $M_1^\pm = 700$  GeV, the width is about 15 GeV. In SM, there is no resonance in  $W^\pm Z$  scattering

The cross section for  $W^\pm Z$  scattering as a function of  $\sqrt{s}$  is shown in Fig. 1 (left panel) in Higgsless models and in two "unitarization models" which attempt to mimic the physics of technicolor type theories, viz., EWCL with Padé approximant or with  $K$ -matrix. Also shown in Fig. 1 (right panel) is the number of events expected in each case with appropriate cuts. It is seen that the Higgsless model can be distinguished with a luminosity of  $300 \text{ fb}^{-1}$  at LHC.

The  $WW$  channel has been examined by Malhotra [8]. The conclusion is that a resonance  $V_1^0$  could be reconstructed with an appropriate luminosity. For example for a resonance mass of 1 TeV a luminosity of  $300 \text{ fb}^{-1}$  would be needed at LHC [8].

### 3. WW scattering at LHC

At a hadron collider like the LHC,  $WW$  scattering can occur with virtual  $W$ 's emitted by the quarks in the hadrons. A  $W$  pair in the final state can be produced either through  $WW$  scattering diagrams, or through  $W$  emission from the partons of the initial hadrons. Fig. 2 shows these two types of contributions. Fig. 2 (a) represents the genuine  $WW$  scattering diagrams, whereas Fig. 2 (b) shows the "Bremsstrahlung" diagrams, which would be a background in the study of  $WW$  scattering.

#### 3.1 Equivalent vector-boson approximation

The equivalent photon approximation (Weizsäcker-Williams approximation) relates the cross section for a charged particle beam to interact with a target with a virtual photon exchange to the cross section for real photon beam to interact with the same target and produce the final state:

$$\sigma = \int dx \sigma_\gamma(x) f_{q/\gamma}(x). \tag{3.1}$$

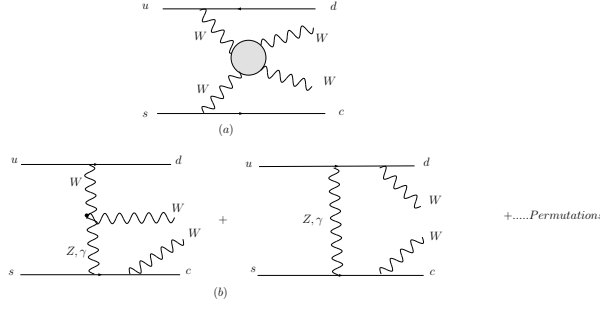


**Figure 2:** Main diagram topologies for the process  $us \rightarrow cdW^+W^-$ . (From [15]).

Here, the photon distribution with momentum fraction  $x$  in a charged-particle beam of energy  $E$  is given by

$$f_{e/\gamma}(x) = \frac{q^2 \alpha}{2\pi x} \ln\left(\frac{E}{m_e}\right) [x + (1-x)^2]. \quad (3.2)$$

This is generalized to what is known as an equivalent (or effective) vector-boson approximation (EVBA) for a process with weak bosons in place of photons [9, 10]. The corresponding distributions of vector bosons  $V$  in a fermion  $f$  are given by

$$\begin{aligned} f_{f/V_{\pm}}(x) &= \frac{\alpha}{2\pi x} \ln\left(\frac{E}{m_V}\right) [(v_f \mp a_f)^2 + (1-x)^2(v_f \pm a_f)^2] \\ f_{f/V_L}(x) &= \frac{\alpha}{\pi x} (1-x) [v_f^2 + a_f^2]. \end{aligned} \quad (3.3)$$

Here the suffixes  $\pm$  on  $V$  denote the helicities  $\pm 1$  of  $V$  and  $V_L$  is the state with helicity 0.

The use of EVBA entails (a) restricting to vector boson scattering diagrams (b) neglecting diagrams of bremsstrahlung type (c) putting on-shell momenta of the vector bosons which take part in the scattering and (d) approximating the total cross section of the process  $f_1 f_2 \rightarrow f_3 f_4 V_3 V_4$  by the convolution of the vector boson luminosities  $\mathcal{L}_{Pol_1 Pol_2}^{V_1 V_2}(x)$  with the on-shell cross section:

$$\begin{aligned} \sigma(f_1 f_2 \rightarrow f_3 f_4 V_3 V_4) &= \int dx \sum_{V_1, V_2} \sum_{pol_1 pol_2} \mathcal{L}_{pol_1 pol_2}^{V_1 V_2}(x) \\ &\times \sigma_{pol}^{on}(V_1 V_2 \rightarrow V_3 V_4, x s_{qq}) \end{aligned} \quad (3.4)$$

Here  $x = M(V_1 V_2)^2 / s_{qq}$ , while  $M(V_1 V_2)$  is the vector boson pair invariant mass and  $s_{qq}$  is the square of the partonic c.m. energy. Note in the context of (c) above that the on-shell point  $q_{1,2}^2 = M_{V_{1,2}}^2$  is outside the physical region  $q_{1,2}^2 \leq 0$ . Thus the extrapolation involved is more than that involved in the case of the equivalent photon approximation.

Even if only the longitudinal polarization, expected to be dominant, is kept, EVBA overestimates the true cross section. The transverse polarization contribution is found to be comparable to the longitudinal one [10]. Improved EVBA [11], going beyond the leading approximation, still overestimates the cross section [12]. Further improvements in EVBA have been attempted [13].

### 3.2 Backgrounds

Backgrounds are of two types:

1. Bremsstrahlung processes – these are processes where the vector bosons are radiated by quark or antiquark partons, and which do not contribute to  $VV$  scattering.

2. Processes which fake a  $VV$  final state.

It is important to understand the first inherent background, and device cuts which may enhance the signal. However, it may be possible to live with it – provided  $VV$  scattering signal is anyway enhanced because it is strong. In that case, one simply makes predictions for the combined process of  $PP \rightarrow VV + X$ . The second background is crucial to take care of, otherwise we do not know if we are seeing a  $VV$  pair in the final state or not.

Background processes are  $q\bar{q} \rightarrow W^+W^-X$ ,  $gg \rightarrow W^+W^-X t\bar{t} + \text{jet}$ , with top decays giving  $W^+W^-$  pair. Electroweak-QCD process  $W^+ + \text{jets}$  can mimic the signal when the invariant mass of the two jets is around  $m_W$ . There is a potential background from QCD processes  $q\bar{q}, gg \rightarrow t\bar{t}X, Wt\bar{b}$  and  $t\bar{t} + \text{jets}$ , in which a  $W$  can come from the decay of  $t$  or  $\bar{t}$ .  $W$  boson pairs produced from the intrinsic electroweak process  $q\bar{q} \rightarrow q\bar{q}W^+W^-$  tend to be transversely polarized. Coupling to  $W^+$  of incoming quark is purely left-handed. Helicity conservation implies that outgoing quark follows the direction of incoming quark for longitudinal  $W$ , and it goes opposite to direction of incoming quark for transverse (left-handed)  $W$ . Hence outgoing quark jet is less forward in background than in signal event, and tagging of the forward jet can help.

In addition, emission in the central region is favoured in the QCD background processes, whereas jet production in the central region is suppressed for  $WW$  scattering. Thus, a veto on additional jets in the central region would be a powerful discriminant between signal and background.

For a discussion of the  $WW$  scattering in the context of LHC detectors, see [14].

### 3.3 Distinguishing the signal

The feasibility of extracting  $WW$  scattering from experiment and comparison of EVBA with exact results was recently studied by Accomando and collaborators [15].

It is known that when  $W$ 's are allowed to be off mass shell, the amplitude grows faster with energy, as compared to when they are on shell [16]. The problem of bad high-energy behaviour of  $WW$  scattering diagrams can be avoided by the use of the axial gauge [17].

Accomando et al. [15] have examined (a) the role of choice of gauge in  $WW$  fusion, in particular, the axial gauge, (b) the reliability of EVBA, (c) the determination of regions of phase space, in suitable gauge, which are dominated by the signal (i.e., the  $WW$  scattering diagrams). Their results show that  $WW$  scattering diagrams do not constitute the dominant contribution in any gauge or phase space region. Thus, there is no substitute to the complete amplitude for studying  $WW$  fusion process at LHC.

The rest of the section contains a description of the results of [15].

Table 1 shows the cross section in different gauges for the contribution of  $us$  partons to the full process  $pp \rightarrow W^+W^-X$ , to only the  $WW$  diagrams, and the ratio of these cross sections. The Higgs boson is assumed to be infinitely heavy. Table 2 shows the same quantities for a Higgs mass of 200 GeV, with a cut on the  $WW$  invariant mass of 300 GeV. It is clear that in both these cases, the  $WW$  contribution is largely cancelled by the ‘‘Bremsstrahlung’’ type background contribution. Even in the axial gauge, in which the  $WW$  contribution is the least, it is still a factor of 2 larger than the actual cross section.

	$\sigma(pb)$		
Gauge	All diagrams	WW diagrams	ratio WW/all
Unitary	$1.86 \cdot 10^{-2}$	6.67	358
Feynman	$1.86 \cdot 10^{-2}$	0.245	13
Axial	$1.86 \cdot 10^{-2}$	$3.71 \cdot 10^{-2}$	2

**Table 1:** No Higgs contribution, using the CTEQ5 Pdf set with scale  $M_W$ . (From [15]).

	$\sigma(pb)$		
Gauge	All diagrams	WW diagrams	ratio WW/all
Unitary	$8.50 \cdot 10^{-3}$	6.5	765
Feynman	$8.50 \cdot 10^{-3}$	0.221	26
Axial	$8.50 \cdot 10^{-3}$	$2.0 \cdot 10^{-2}$	2.3

**Table 2:**  $M_h=200$  GeV Higgs and  $M(WW) > 300$  GeV . (From [15]).

The  $WW$  invariant-mass distributions are also obtained in [15]. Again, the result including all diagrams does not give a true representation of the  $WW$  contribution alone.

Fig. 3 shows a comparison of the  $WW$  invariant mass distribution  $M(WW)$  for the process  $us \rightarrow dcW^+W^-$  in an improved EVBA with the exact complete result for the two cases of a very heavy Higgs and a Higgs of mass 250 GeV. EVBA exceeds the exact result except at the Higgs resonance.

Accomando et al. [15] also investigate the total cross section in EVBA and exact computation and their ratio for different cuts on the  $W$  scattering angle. The angular cuts serve to decrease the discrepancy between EVBA and exact computation.

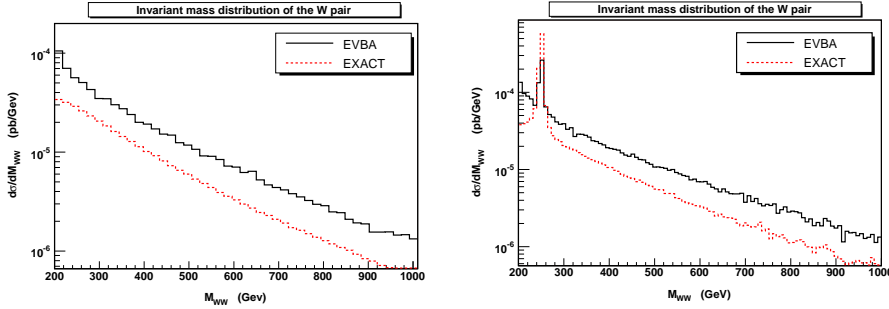


**Figure 3:**  $WW$  invariant mass distribution  $M(WW)$  for the process  $us \rightarrow dcW^+W^-$  with EVBA (black solid curve) and with exact complete computation (red dashed curve) for no Higgs (left) and  $M_h=250$  GeV (right). (From [15]).

The  $WW$  invariant mass distribution in the process  $PP \rightarrow us \rightarrow cdW^+W^-$  is shown in Fig. 3.3, imposing the cuts shown in Table 3. It is seen that for sufficiently large  $WW$  invariant mass it seems feasible to distinguish between light Higgs and heavy Higgs scenarios. It is reasonable to

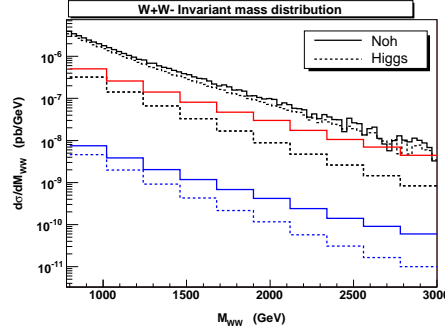


**Figure 4:** The  $WW$  invariant mass distribution in  $PP \rightarrow us \rightarrow cdW^+W^-$  for no Higgs (solid curves) and for  $M_h=200$  GeV (dashed curve). The two intermediate (red) curves are obtained imposing cuts shown below. The two lowest (blue) curves refer to the process  $PP \rightarrow us \rightarrow cd\mu^-\bar{\nu}_\mu e^+ \nu_e$  with further acceptance cuts:  $E_l > 20$  GeV,  $p_T > 10$  GeV,  $|\eta_l| < 3$ .

$E(\text{quarks}) > 20$ GeV
$P_T(\text{quarks}, W) > 10$ GeV
$2 <  \eta(\text{quark})  < 6.5$
$ \eta(W)  < 3$

**Table 3:** The selection selection cuts applied in the above figure

anticipate that this is the kinematic region where it may be possible to test non-standard scenarios of symmetry breaking.

#### 4. Summary

In the absence of a light Higgs,  $WW$  interactions become strong at TeV scales. Study of  $WW$  scattering can give information of the electroweak symmetry breaking sector and discriminate between models. In general there are large cancellations between the scattering and bremsstrahlung diagrams. Hence extraction of  $WW$  scattering contribution from the process  $PP \rightarrow W^+W^-X$  needs considerable effort. EVBA overestimates the magnitude in most kinematic distributions. Cuts to reduce background were discussed. It is possible to extract information on  $WW$  scattering from hadronic experiments by concentrating on the large-invariant mass region.

#### References

- [1] J. M. Cornwall, D. N. Levin and G. Tiktopoulos, *Derivation of gauge invariance from high-energy unitarity bounds on the S matrix*, *Phys. Rev. D* **10** (1974) 1145, *ibid* **11** (1975) 972 (E);  
 C. E. Vayonakis, *Born helicity amplitudes and cross-sections in nonabelian gauge theories*, *Lett. Nuovo Cim.* **17** (1976) 383; B. W. Lee, C. Quigg and H. B. Thacker, *Weak interactions at very high-Energies: the role of the Higgs boson mass*, *Phys. Rev. D* **16** (1977) 1519; D. A. Dicus and V. S. Mathur, *Upper bounds on the values of masses in unified gauge theories*, *Phys. Rev. D* **7** (1973) 3111; M. S. Chanowitz and M. K. Gaillard, *The Tev physics of strongly interacting W's and Z's*, *Nucl. Phys. B* **261** (1985) 379; H. G. J. Veltman, *The equivalence theorem*, *Phys. Rev. D* **41** (1990) 2294.

- [2] S. Weinberg, *Nonlinear realizations of chiral symmetry*, *Phys. Rev.* **166** (1968) 1568.
- [3] T. Appelquist and C. W. Bernard, *Strongly interacting Higgs bosons*, *Phys. Rev. D* **22** (1980) 200; A. C. Longhitano, *Low-energy impact of a heavy Higgs boson sector*, *Nucl. Phys. B* **188** (1981) 118; *Phys. Rev. D* **22** (1980) 11.
- [4] A. Dobado, M. J. Herrero and J. Terron, *The role of chiral Lagrangians in strongly interacting  $W_L W_L$  signals at  $PP$  supercolliders*, *Z. Phys. C* **50** (1991) 205;
- [5] C. Csaki, C. Grojean, H. Murayama, L. Pilo and J. Terning, *Gauge theories on an interval: Unitarity without a Higgs*, *Phys. Rev. D* **69** (2004) 70 [hep-ph/0305237]; C. Csaki, C. Grojean, L. Pilo and J. Terning, *Towards a realistic model of Higgsless electroweak symmetry breaking*, *Phys. Rev. Lett.* **92** (2004) 101802 [hep-ph/0308038].
- [6] Y. Nomura, *Higgsless theory of electroweak symmetry breaking from warped space*, *JHEP* **11** (2003) 050 [arXiv:hep-ph/0309189].
- [7] A. Birkedal, K. Matchev and M. Perelstein, *Collider phenomenology of the Higgsless models*, *Phys. Rev. Lett.* **94** (2005) 191803 [hep-ph/0412278].
- [8] R. Malhotra, *W W fusion in Higgsless models*, hep-ph/0611380.
- [9] S. Dawson, *The effective W approximation*, *Nucl. Phys. B* **249** (1985) 42; G. L. Kane, W. W. Repko and W. B. Rolnick, *The effective  $W^\pm$ ,  $Z^0$  approximation for high-energy collisions*, *Phys. Lett. B* **148** (1984) 367; J. Lindfors, *Distribution functions for heavy vector bosons inside colliding particle beams*, *Z. Phys. C* **28** (1985) 427.
- [10] R. M. Godbole and S. D. Rindani, *Intermediate mass Higgs boson production and the equivalent vector boson approximation*, *Phys. Lett. B* **190** (1987) 192; *The equivalent vector boson approximation for intermediate mass Higgs boson production*, *Zeit. Phys. C* **36** (1987) 395.
- [11] P. W. Johnson, F. I. Olness, and W.-K. Tung, *The effective vector boson method for high-energy collisions*, *Phys. Rev. D* **36** (1987) 291.
- [12] R. M. Godbole and F. I. Olness, *Contribution of transverse gauge bosons to Higgs production and the equivalent vector boson approximation*, *Int. J. Mod. Phys. A* **2** (1987) 1025.
- [13] I. Kuss and H. Spiesberger, *Luminosities for vector boson - vector boson scattering at high-energy colliders*, *Phys. Rev. D* **53** (1996) 6078 [arXiv:hep-ph/9507204].
- [14] ATLAS Collaboration, *ATLAS detector and physics performance. Technical design report. Vol. 2*, CERN/LHCC/99-15; CMS Collaboration, *CMS, the Compact Muon Solenoid: Technical proposal*, CERN/LHCC/94-38.
- [15] E. Accomando, A. Ballestrero, A. Belhouari and E. Maina, *Isolating vector boson scattering at the LHC: Gauge cancellations and the equivalent vector boson approximation vs complete calculations*, *Phys. Rev. D* **74** (2006) 073010 [arXiv:hep-ph/0608019].
- [16] R. Kleiss and W. J. Stirling, *Anomalous high-energy behavior in boson fusion*, *Phys. Lett. B* **182** (1986) 75.
- [17] Z. Kunszt and D. E. Soper, *On the validity of the effective W approximation*, *Nucl. Phys. B* **296** (1988) 253.